# Lab on a Chip

Miniaturisation for chemistry, physics, biology, & bioengineering

www.rsc.org/loc

Volume 9 | Number 24 | 21 December 2009 | Pages 3453–3608

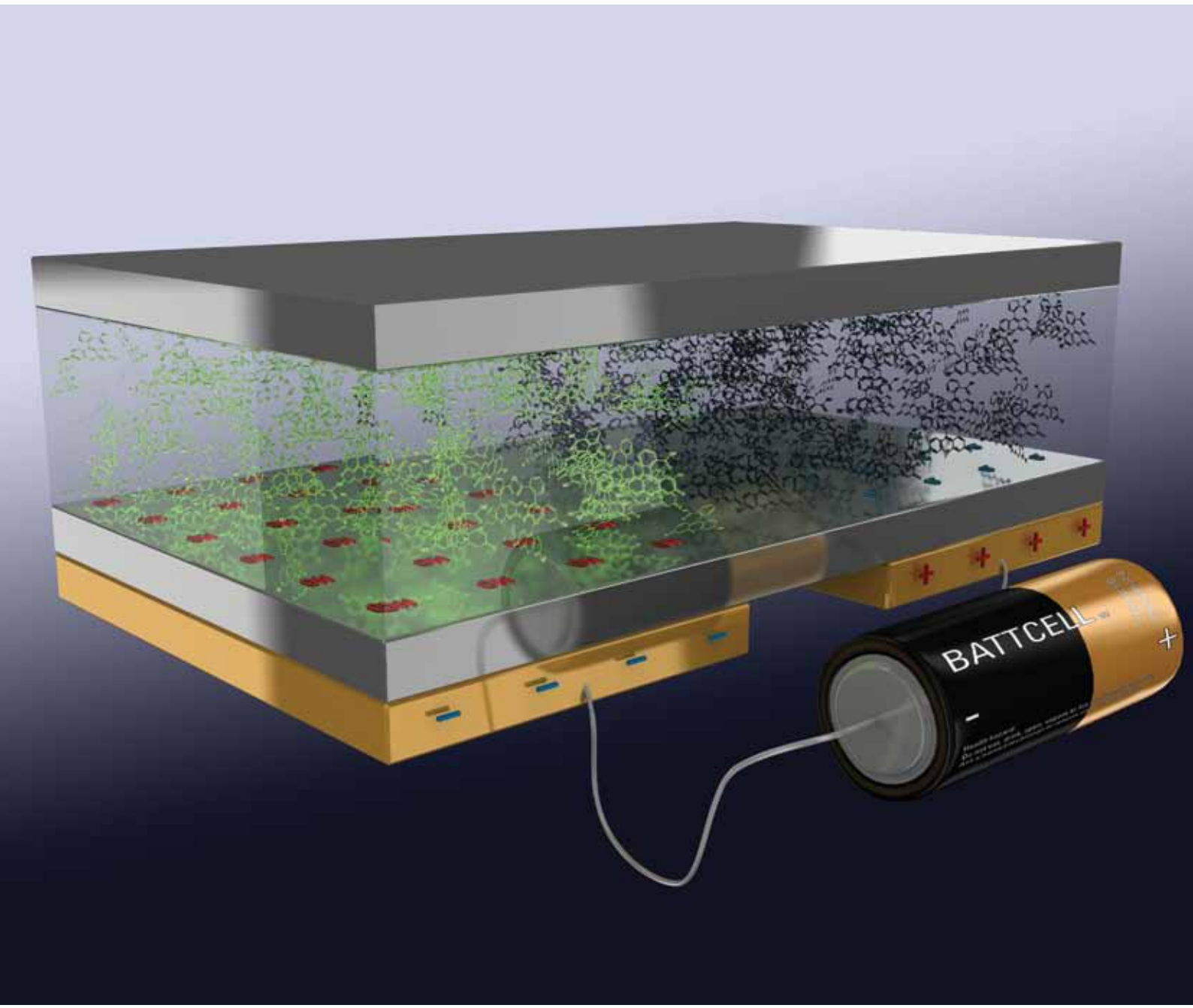


ISSN 1473-0197



RSC Publishing

# Field-effect based attomole titrations in nanoconfinement

**Rogier B. H. Veenhuis, Egbert J. van der Wouden, Jan W. van Nieuwkasteele, Albert van den Berg and Jan C. T. Eijkel***

*Received 6th July 2009, Accepted 25th September 2009*
*First published as an Advance Article on the web 16th October 2009*
**DOI: 10.1039/b913384d**

This paper describes a novel capacitive method to change the pH in micro- and nanofluidic channels. A device with two metal gate electrodes outside an insulating channel wall is used for this purpose. The device is operated at high ionic strength with thin double layers. We demonstrate that gate potentials applied between the electrodes cause a release or uptake of protons from the silicon nitride surface groups, resulting in a pH shift in the channel and a titration of solution compounds present. Due to the high quality silicon nitride insulating layer, the effect is purely capacitive and electrolysis can be neglected. Fluorescein was employed as a fluorescent pH indicator to quantify the induced pH changes, and a maximum change of 1.6 pH units was calculated. A linear relationship was found between applied potential and fluorescein intensity change, indicating a linear relation between actuated proton amount and applied voltage. Since this pH actuation method avoids redox reactions and can be operated at physiological ionic strength, it can be very useful as a "soft" way to change the pH in very small volumes *e.g.* in bioassays or cell-based research. The sensitivity of the optical detection method poses the only limit to the detectable amount of substance and the observed volume. In a preliminary measurement we show one possible application, namely titration of 100 attomol of TRIS in a 7 pL detection volume. It is important to stress that this pH actuation principle fundamentally differs from the pH changes occurring in ionic transistors which are due to counterion enrichment and coion exclusion, because it does not rely on double-layer overlap. As a result it can be operated at high ionic strength and in channels of up to at least 1 μm height.

## Introduction

Lab-on-a-chip technologies are widely applied in analytical, chemical, biological and sensor and actuator systems. When downscaling lab-on-a-chip devices, the surface to volume ratio increases and surface properties become increasingly important for system behavior.[1] Surface charge governed phenomena in particular are important, so that control of the channel wall charge is crucial in nanofluidic separation and concentration processes.[2–4] Glass is often used as a substrate to fabricate fluidic channels due to its favorable properties: it is chemically inert, optically transparent and provides good electrical insulation. Glass channel walls, however, also have a strongly pH- and ionic strength-dependent surface charge, with a point of zero charge (PZC) at pH $\approx$ 3 and a negative surface charge at higher pH values, resulting from deprotonation of surface silanol groups.[2] The surface silanol groups furthermore provide a large proton buffer capacity at pH values away from the PZC.

Recently the influence of the buffer capacitance of a silicon oxide channel wall on the solution pH in a nanochannel was demonstrated.[3] A strong release of protons from the walls was shown to occur during capillary filling. It was argued that such a proton release or uptake would occur in any transient situation, such as a change of the solvent properties or ionic strength. Since the effect scales with the surface area, its relevance increases with downscaling. Here we demonstrate a method of externally controlling this proton release or uptake. The surface charge on glass channel walls is normally exclusively determined by the chemical environment of the solution, but can also be modified electrically through the application of an electrical potential difference between an electrode outside the channel wall and the filling solution. This so-called voltage gating process has, for example, been used to modify the electroosmotic flow in a channel in flowFETs or its ion permselectivity in ionic transistors.[4,5]

Fig. 1 shows a schematic layout of the chip, which consists of an 860 nm deep fluidic channel enclosed on one side by a 360 nm thick silicon nitride layer and on the other side by a glass wafer, with 2 silicon gate electrodes deposited on the silicon nitride layer. Fig. 1 also schematically shows the capacitive proton actuation method used. We will theoretically show that capacitive proton actuation will occur whenever the insulating wall has a proton buffer capacitance, and quantify this amount.[6] We also experimentally demonstrate that by using a high quality dielectric as an insulating layer, leakage currents can be minimized so that the pH actuation mechanism is purely capacitive.

The proton release considered here and the resulting pH changes should be distinguished well from another phenomenon that occurs exclusively in nanochannels at low salt concentration. In nanochannels with double-layer overlap and a negatively charged wall, the average pH is significantly lower than the pH in connecting reservoirs due to counterion enrichment of the protons, as described by the Boltzmann equilibrium distribution.[7] The pH change we investigate here on the other hand is a transient and non-equilibrium effect related to a change of electrochemical equilibrium at the glass walls and occurs at all

*MESA+ Institute for Nanotechnology, Universiteit Twente, The Netherlands. E-mail: j.c.t.eijkel@utwente.nl*

 

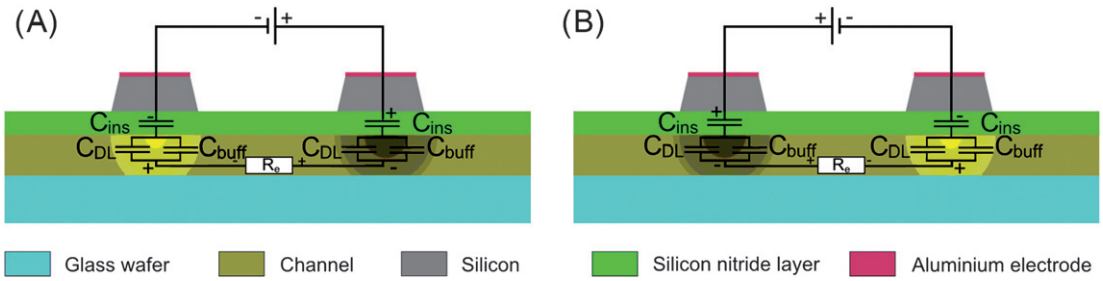


**Fig. 1** The principle of capacitive pH actuation. (A) Solution acidification occurs under the right (positive) electrode and basification under the left electrode. (B) When the voltage is reversed, acidification occurs under the left (positive) electrode and basification under the right electrode. Basification and acidification can be observed by an increase and decrease of the pH-dependent fluorescence intensity of fluorescein. $C_{ins}$: insulator capacitance; $C_{DL}$: double-layer capacitance; $C_{buff}$: buffer capacitance of the silicon nitride surface and $R_e$: electrolyte resistance.

salt concentrations. It is based on the proton buffer capacity of the glass walls. The effects of proton buffering surface groups on an insulating surface have been recognized mainly in the field of radial voltage control in capillary electrophoresis[8,9] and field-effect flow control (FEFC).[5,10] However, in these situations these effects were considered to be a limitation in terms of pH operating window, rather than an opportunity for pH actuation. Measurements with FEFC-type devices using capacitive gates recently showed indications for both Faradaic and capacitive proton generation, however, the behavior was not analyzed.[11,7]

Capacitive pH actuation in micro- and nanosystems forms an addition to Faradaic (electrolysis-based) pH actuation in microsystems, which especially in a sensor–actuator pair with an ISFET has been used to determine the buffer capacity of solutions.[12–14] In Faradaic proton actuation much larger proton amounts can be actuated, but inevitably accompanied by other electrochemical reactions and possibly gas bubble formation due to the electrolysis.

External pH control in a confined fluidic system at physiological salt strengths would be highly convenient for instance for detection or for the application of external stimuli to cells or biological systems. At present this is possible only by convection which is cumbersome, axial diffusion which is slow, or electrolysis which leads to unwanted side products like hydrogen and oxygen gas evolution.[7] The capacitive coupling between surface proton charge and gate potential we use is the same as that used for pH sensing in ion-sensitive field-effect transistors (ISFETs).[15,16] However, where the ISFET measures the gate insulator/electrolyte interfacial potential as a function of the pH of the bulk electrolyte, in capacitive pH actuation the electrolyte pH is controlled by modifying the gate insulator/electrolyte potential.

## Theory

### The insulator/electrolyte interface

At a solid/liquid interface most materials develop a surface charge due to ionizing surface groups. This charge is screened by an equal amount of oppositely charged ions from the solution, forming the electrical double layer (EDL) with a characteristic length given by the Debye length.[17,18] In most models the EDL is further differentiated into a Stern layer that is composed of immobilized charges near the surface and a diffuse layer in which ions can freely diffuse.

The device as shown in Fig. 1 enables capacitive modification of the surface potential. This control over the surface potential by means of an external bias potential can be modeled in the electrical domain with a 3 capacitor circuit where 2 capacitors represent the Stern and diffuse layer capacitance and one capacitor the insulating nitride layer capacitance.[5,19] The Stern layer and diffuse layer capacitance can furthermore be combined in the double-layer capacitance, simplifying the model to two capacitors in series (see Fig. 2A and B). However, it is often not recognized that the application of this model is limited to situations where the insulator surface is chemically inert. Whenever the surface is capable of dissociating or binding protons, induced changes in the surface proton concentration will be buffered by these surface groups. In this case charge is not stored on the EDL capacitance by non-surface binding cations (generating a surface potential change) but on the surface proton buffer capacitance as protons, generating a change of surface charge (see Fig. 2C). The fraction of capacitively induced charges that binds to the surface as protons will be shown to depend on the ratio between the capacitance of the EDL and the surface proton buffer capacitance.[2] To describe this process, the equivalent circuit has to be extended with an extra capacitance representing the chemical proton buffer capacitance of the surface groups, in parallel to the EDL capacitance. Fig. 2 sketches these 3 situations for a solid/liquid interface with an external insulated electrode, Fig. 2A the equilibrium situation without an applied bias potential for a pH > $pH_{pzc}$, Fig. 2B for a negative applied bias potential while no proton-binding groups are present at the surface, and Fig. 2C the situation when proton buffering surface groups are present.

### Electrical model

Fig. 3 provides the electrical equivalent circuits of this chip design in more detail. The left-hand side of Fig. 3 gives a dynamic equivalent model including both resistive and capacitive elements.[20] Since the chip layout consists of 2 similar electrolyte/insulator/silicon interfaces, the system is symmetric around the electrolyte resistance $R_e$. The insulator capacitance $C_{ins}$, double-layer capacitance $C_{DL}$ and surface proton buffer capacitance $C_{buff}$ were already introduced in the previous section. The impedance $Z_s$ represents the silicon gate capacitance. At large bias potentials depletion or accumulation effects can arise in the p-type silicon resulting in space charge regions at the silicon insulator interface. The proton buffer capacitance of the surface

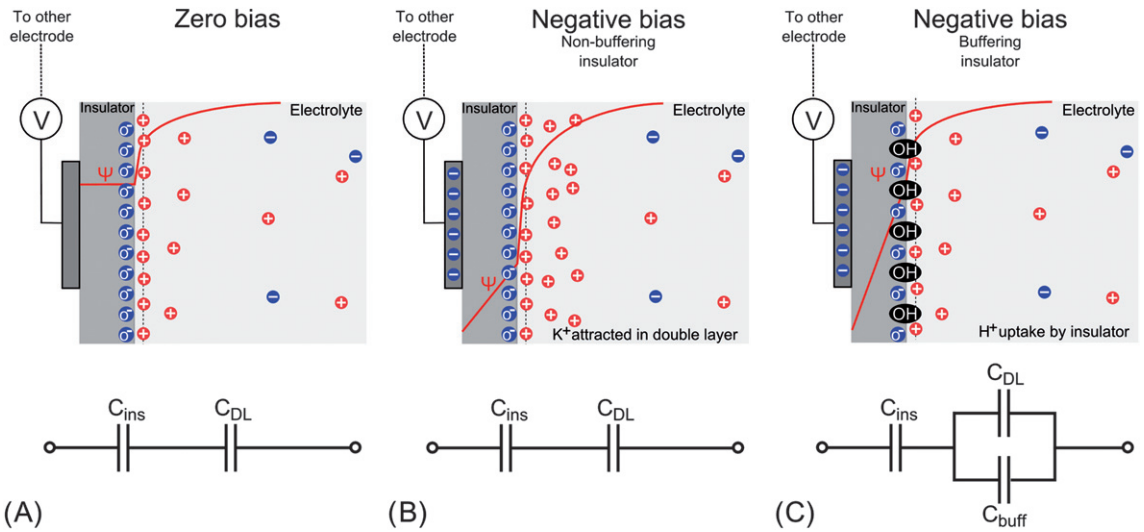


**Fig. 2** Mechanism and simplified equivalent electrical circuits of capacitive actuator devices. (A) At zero bias, a negative surface charge is assumed due to the presence of $O^-$ groups, and an equal but opposite charge (for simplicity represented by only $K^+$ ions) resides in the solution. (B) At negative bias and a non-proton buffering insulator surface, extra counterion charge is attracted in the electrical double-layer. (C) At negative bias and a proton buffering insulator surface, additionally attracted protons are buffered by association with the $O^-$ surface groups to form OH groups, decreasing the surface charge density. When the buffer capacity is high with respect to the double-layer capacitance, the surface potential will not change.

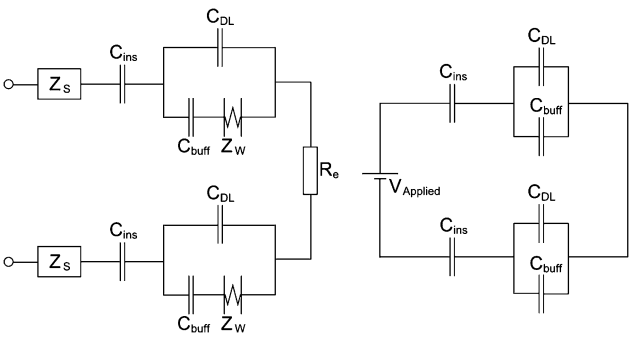


**Fig. 3** Equivalent electrical circuit of the pH actuation chip. The left side represents a dynamic equivalent circuit and the right side illustrates a simplified model for the steady state situation.

groups $C_{buff}$ is connected in series with the Warburg impedance $Z_w$ that models the solution diffusion resistance for protons. In this circuit the double-layer capacitance is charged with non-surface binding ions such as potassium and chloride. The buffer capacitance is charged exclusively by protons. The model neglects proton diffusion transport in the axial direction of the channel. This is justified at the experimental time scale of 1 s, since the time constant of axial diffusion is more than 100 s. The model could furthermore be extended by adding a parasitic capacitance to account for capacitive coupling to the environment.

In the steady state situation the capacitors in the system are charged and the current equals zero. The potential differences across the electrolyte resistance, silicon layer and the Warburg impedance as a consequence are zero. Under these conditions the circuit can be simplified to the equivalent circuit in the right-hand side of Fig. 3. This purely capacitive circuit can be used to determine the relation between the applied actuation voltage and the final number of protons dissociated from the wall surface.

To calculate the number of protons released as a function of the applied potential, $C_{ins}$, $C_{DL}$ and $C_{buff}$ have to be determined. The capacitance of the insulator (F $m^{-2}$) is

$$C_{ins} = \frac{\varepsilon_0 \varepsilon_r}{d} \quad (1)$$

where $\varepsilon_0$ (F $m^{-1}$) and $\varepsilon_r$ represent the permittivity of vacuum and the insulating material, respectively, and $d$ (m) the thickness of the insulating layer. The double-layer capacitance is calculated from the series addition of the Stern capacitance $C_{Stern}$ (F $m^{-2}$) and the diffuse layer capacitance. We find for the differential double-layer capacitance $C_{DL}$ (F $m^{-2}$)

$$\frac{1}{C_{DL}} = \frac{1}{C_{Stern}} + \frac{1}{\left(\frac{\varepsilon\varepsilon_0 q^2 n^0}{kT}\right)^{1/2} \cosh\left(\frac{q\phi_2}{2kT}\right)} \quad (2)$$

where $\phi_2$ (V) is the electrical potential at the Stern plane, $q$ the unit charge ($1.6 \times 10^{-19}$ C), $n^0$ ($m^{-3}$) the ion number density in the electroneutral bulk solution, $k$ the Boltzmann's constant ($1.38 \times 10^{-23}$ J $K^{-1}$) and $T$ (K) the absolute temperature.[18]

The electrical equivalent of the nitride buffer capacitance is derived as follows. When the channel is filled with solution, a surface charge arises at the solid/liquid interface originating from the amphoteric site dissociation of silanol groups and the single site dissociation of basic amino sites that are both present at the silicon nitride surface.[21]

$$[SiOH_2] \Leftrightarrow [SiOH] + [H^+]_S \quad (3)$$

$$[SiOH] \Leftrightarrow [SiO^-] + [H^+]_S \quad (4)$$

$$[SiNH_3] \Leftrightarrow [SiNH_2] + [H^+]_S \quad (5)$$

Here $[H^+]_s$ is the proton concentration at the wall surface, related to the proton concentration in the electroneutral bulk *via* the Boltzmann equation. The equilibrium constants for reactions

(3)–(5) are typically taken as $pK_b = -2$ (3), $pK_a = 6$ (4) and $pK_b = 4.75$ (5). The surface charge will depend on the pH of the bulk solution and the ratio of amino to silanol surface groups. For the low-pressure chemical vapor deposition (LPCVD) silicon nitride used here, the PZC is expected to be around pH 4 and the ratio of amino to silanol surface groups to be about 0.02.[22–24] Due to the three reactions given above, the surface will possess an intrinsic (chemical) buffer capacitance $\beta$ (groups per $m^2$) for protons. This can be converted to an electrical analogue $C_{buff}$ (F $m^{-2}$) as described in ref. 9,

$$C_{buff} = \frac{q^2\beta}{2.3kT} \quad (6)$$

Due to the low ratio of amino to silanol groups, the intrinsic buffer capacitance of the silicon nitride at pH = 6.9 in a 0.01 M electrolyte solution can be assumed to be approximately equal to that of a silicon oxide surface which is approximately $4 \times 10^{17}$ groups per $m^2$,[9] resulting in $C_{buff} = 1.1$ F $m^{-2}$.

The amount of protons theoretically released from the silicon nitride wall, $N_{H,theory}$ (C $m^{-2}$), can now be obtained by applying electrical network theory to the right-hand side circuit of Fig. 3.† Assuming that $C_{ins} \ll C_{DL}$,

$$N_{H,theory} = VC_{ins}\frac{C_{Buff}}{(C_{Buff} + C_{DL})} \quad (7)$$

where $C_{ins}$ equals $1.96 \times 10^{-4}$ F $m^{-2}$, using the parameter values listed in Table 1. It can be seen that the released amount of protons is expected to be directly proportional to the applied voltage. The equation shows that the proton actuation process is most efficient when $C_{buff} \gg C_{DL}$. In that case all charge is stored as surface-bound charge and actuated or taken up as protons. The value for $C_{buff}$ derived above was 1.1 F $m^{-2}$. For $C_{DL}$ a value of 0.35 F $m^{-2}$ can be obtained for a 0.01 M KCl solution and assuming a Stern layer capacitance of 0.8 F $m^{-2}$.[9] For the last factor of eqn (7) we thus obtain 0.76.

Released protons will protonate fluorescein molecules, increasing the concentration of the non-fluorescent monoanion and decreasing the concentration of the fluorescent dianion, the reaction of which has a $pK_a$ of 6.7.[25] Close to the $pK_a$, fluorescence intensity changes will provide the most sensitive indication of pH changes.

Experimentally, the amount of released protons can be derived from fluorescence intensity measurements. In the pH region where the fluorescein buffer capacity is much larger than the buffer capacity of protons or hydroxyl ions (which at a fluorescein concentration of 0.1 mM is between $5.5 < pH < 7.5$), every proton released or taken up will decrease or increase the fluorescence intensity with an amount equal to the intensity difference between mono- and dianion. The experimentally determined value for the amount of released protons $N_{H,expt}$ (C $m^{-2}$) therefore is

$$N_{H,expt} = \frac{-q\Delta I}{A(F_{dianion} - F_{anion})} \quad (8)$$

† The charge on the insulator capacitance which equals $V \times C_{ins}$ must be equal to the charge on the double-layer and buffer capacitance combined. Of this charge, the fraction on the buffer capacitance equals $C_{buff}/(C_{buff} + C_{DL})$.

**Table 1** Parameter values for calculating RC time constant

| Parameter | Value |
|---|---|
| $l_e$ | $4.6 \times 10^{-3}$ m |
| $l_g$ | $3.6 \times 10^{-3}$ m |
| $\varepsilon_0$ | $8.85 \times 10^{-12}$ F $m^{-1}$ |
| $\varepsilon_r$ | 8[27] |
| $\sigma_e$ | 0.1585 S $m^{-1}$ |
| $d$ | 360 nm |
| $h$ | 860 nm |

where $q$ is the unit charge ($1.6 \times 10^{-19}$ C), $\Delta I$ (a.u.) the observed change in fluorescence intensity, $A$ the observed area, and $F_{dianion}$ and $F_{anion}$ (a.u. per molecule) the fluorescence intensity of a fluorescein dianion and monoanion molecule in our system, respectively. The change in fluorescence intensity will therefore be directly proportional to the released amount of protons. It should be noted that in this analysis the proton uptake of the glass wall opposite to the silicon nitride wall has not been taken into account.

The actuation speed that can be obtained is limited by several time constants in the system. Assuming that the chemical reaction rates are infinitely fast, the two main contributions are the electrical RC time for the charging of the electrical double-layer and the time constant for proton diffusion across the channel height. The time constant for proton diffusion across the channel, calculated from the proton diffusion constant $D$ and the channel height $h$ as $h^2/2D$, is 40 μs. The electrical RC time is determined by the series circuit consisting of twice the insulating layer capacitance and the resistance of the connecting fluidic channel (Fig. 3)[26] and can be approximated by

$$t_{RC} = R_e C_{ins} = \frac{1}{\sigma_e}\frac{l_e}{wh}\frac{\varepsilon_0\varepsilon_r l_g w}{2d} = \frac{l_e l_g \varepsilon_0 \varepsilon_r}{2\sigma_e hd} \quad (9)$$

where $\sigma_e$ is the electrolyte conductivity, $l_e$ the center distance between two planar gate electrodes, $l_g$ the length of the gate electrode, and $w$ the summated width of all channels. The factor 2 in the denominator derives from the presence of two capacitors in series. The parameters determining the time constant are listed in Table 1. Based on these values a time constant of 12 ms is calculated.

After actuation, a pH gradient will exist in the longitudinal direction of the channel, leading to axial diffusion of protons and equilibration. The time constant for this process depends on the length of the gate electrode $l_g$ and the proton diffusion coefficient $D$ as $l_g^2/2D$ and is about 1000 s in the present chip.

## Experimental

### Devices

The pH actuation chip was fabricated by a sequence of thin film deposition, etching and annealing steps, using a procedure published before.[8] An overview of the fabrication process is given in Fig. 4. The chip consists of a Pyrex substrate with patterned silicon gate electrodes and fluid reservoirs. LPCVD silicon nitride is used as an insulating layer due to its favorable insulating properties and high dielectric constant.[28] The channels have a height of 860 nm and a total length of 12 mm. An

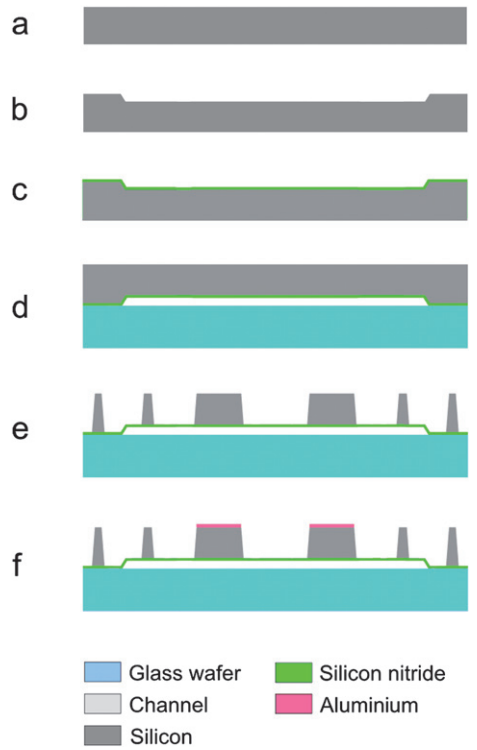


**Fig. 4** Fabrication process: (a) a native oxide is grown on a p-type single sided polished wafer (orientation ⟨1,0,0⟩), (b) channels are created using reactive ion etching (RIE), (c) a 360 nm layer of low stress $Si_3N_4$ is deposited using LPCVD, (d) the silicon substrate is anodically bonded to a Pyrex wafer, (e) fluid reservoirs and gate electrodes are created by selective wet etching of the silicon wafer, (f) aluminium electrode pads (1 μm thickness) are sputtered and annealed to lower the contact resistance.

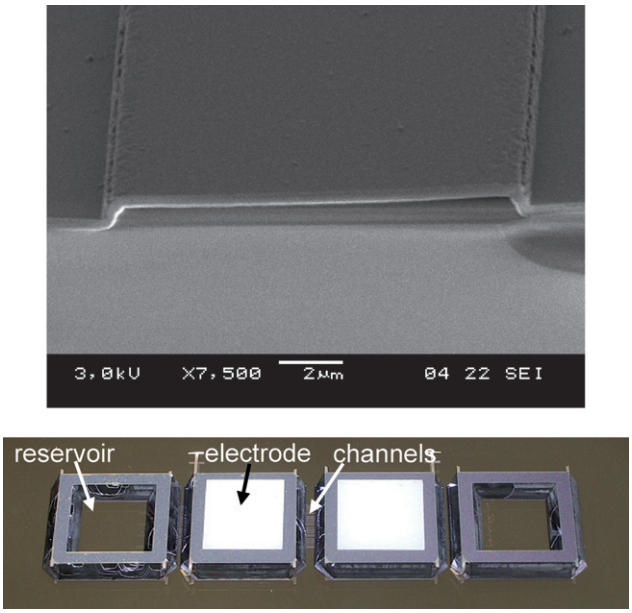


**Fig. 5** (Top) SEM image of a cross-section of one channel, showing the 360 nm silicon nitride capping layer and a channel with a height of 860 nm and a width of 15 μm. (Bottom) Image of a pH actuation chip with on the left and right 2 patterned silicon reservoirs connected by fluidic channels, and in between 2 silicon gate electrodes covered with 1 μm aluminium.

array of five channels connects the reservoirs, with widths of 5, 10, 15, 20 and 100 μm. The silicon wafer was annealed at 1000 °C after silicon nitride deposition to oxidize the surface and increase the number of SiOH groups at the surface. A picture of a complete device and a SEM image of a channel are shown in Fig. 5.

## Experimental setup

Electrical actuation potentials were applied with a Keithley 2410 sourcemeter interfaced to a computer by GPIB-USB and interfaced to the gate electrodes by probe needles. The glass substrate was electrically floating. Currents during actuation were measured using a Keithley 6485 Picoammeter. Fluorescent microscopy was performed in a dark room using a Leica DM IRM inverted microscope with a 63× NA = 0.7 objective and an I3 filter cube illuminated with a mercury lamp. The area illuminated by the mercury lamp was reduced with a diaphragm to fit the region of interest, in this way reducing the influence of photobleaching and minimizing the generation of leakage currents due to light-induced photocurrents.[29] For observation a region was chosen under a gate electrode directly bordering the gap between the gate electrodes. The fluorescent emission was monitored with a photomultiplier tube (Hamamatsu PMT 7422-02) with a sample frequency of 50 Hz. The photomultiplier tube was interfaced to a computer using a National Instruments NI USB-6008 12 bit analog-to-digital converter and accompanying software tool. Alternatively, an Andor iXon EMCCD camera was employed for visualization.

## Measurement protocol

The fabrication process yields completely closed insulated channels. Prior to the measurements the silicon nitride capping layers were scratched open inside the fluid reservoirs and subsequently filled with measuring solution by capillary force. Measurements were performed in solutions containing 10 mM KCl in deionized water and 100 μM fluorescein (pH 6.9) as a pH indicator with excitation wavelength 494 nm and emission wavelength 521 nm. Titration experiments were performed in a solution containing 10 mM KCl in deionized water, 100 μM fluorescein Na and 100 μM TRIS ($pK_a$ 8.2 at 20 °C). All chemicals were obtained from Sigma Aldrich.

One electrode was kept grounded while to the second electrode an alternating potential bias was applied, symmetrical around ground. The solution was left electrically floating. Assuming equal partitioning of the applied potential bias over both insulator capacitances, an applied square wave amplitude of $A$ V results in twice an $A/2$ V potential drop over the insulator capacitances. Frequency and voltage amplitude were varied for the different experiments. The potential bias mentioned in the text is always the amplitude of the applied signal waveform ($A$ V), twice the single electrode bias. The actuation starts with a positive applied bias on the electrode above the observed area. Following data acquisition, image processing and data analysis were performed in Matlab.

### Breakdown field of the silicon nitride insulating layer

The maximum potential that can be applied during actuations is determined by the breakdown field of the insulating layer. The breakdown field of the silicon nitride layer was determined under positive and negative bias potential through a film of the same thickness as the channel wall, sandwiched between the silicon wafer and a 1 μm thick aluminium electrode. The breakdown field was studied by stepping the bias potentials with increments of 1.0 V $s^{-1}$. For a negative and positive bias the breakdown field was determined to be −0.6 V $nm^{-1}$ and 0.8 V $nm^{-1}$, respectively.

## Results and discussion

### Leakage currents

To assure a capacitive pH modulation, leakage currents through the silicon nitride film, leading to electrolysis of water, have to be negligible compared to capacitively induced currents. Fig. 6 shows typical transient currents measured during application of a potential difference between both gates starting at $t = 5$ s, for applied bias potentials of −30, −20, −10, 10, 20, and 30 V (the plus sign was arbitrarily assigned to one polarity). All current transients show similar behavior, with an initial exponential decrease (time constant approximately 0.35 s) indicating capacitive charging, followed by a steady state indicating a leakage current through the silicon nitride thin film.

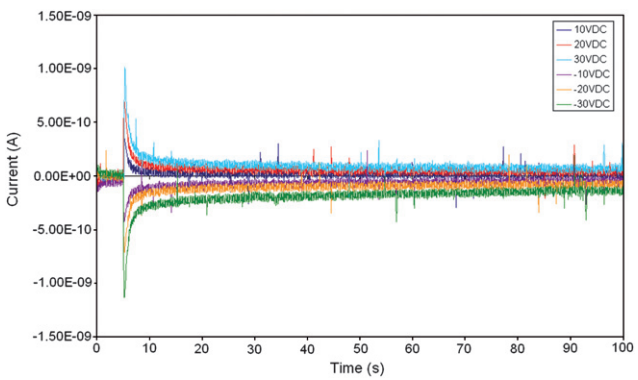


**Fig. 6** Transient currents measured during application of DC gate potentials for positive and negative biases.

The leakage currents through the insulating layer show an asymmetry towards the applied potential. For negative biases a slightly larger leakage current is observed, possibly due to an asymmetry in incorporated trapping sites inside the SiN films under the two gate electrodes during deposition, which can lead to a bias-dependent leakage current.[28] Within the voltage range applied a linear dependence of the leakage current on the actuation voltage was found, with the current at negative bias increasing with 5 pA $V^{-1}$ and the current at positive bias increasing with 2.4 pA $V^{-1}$. At the highest applied negative bias of −25 V this corresponds to a current of −125 pA, corresponding to −18 nA $cm^{-2}$. When it is assumed that the leakage currents entirely lead to electrochemical decomposition of water, the amount of actuated protons during 1 s is $1.8 \times 10^{-4}$ C $m^{-2}$. From eqn (7) the amount of capacitively actuated protons is calculated as $4.5 \times 10^{-3}$ C $m^{-2}$, using the values of $C_{buff}$ and $C_{DL}$ mentioned for complete capacitor charging. Faradaic actuation is therefore expected to account for less than 4% of the observed protonation effects during a 1 s actuation period at 25 V applied voltage. To assure that the proton actuation due to Faradaic current was negligible in the titration experiments, maximum bias voltages of −25 and 25 V were therefore applied and a pulse duration of maximally 1 s. In experiments to investigate the leakage current influence, longer pulse durations were, however, applied.

### Proton actuation and fluorescein titration

Fig. 7 shows two 3-dimensional plots of the fluorescence intensity in the channel, obtained from photomicrographs during actuation with an alternating bias on both gate electrodes of 10/−10 V in a solution containing 0.1 mM fluorescein. In the two plots the bias is reversed, and it can clearly be seen that each time the fluorescence decreases in the area above the positively biased electrode. Only small changes in the fluorescence intensity in the inter-electrode gap were found, indicating the potential of this method to locally influence the pH.

To demonstrate that the pH actuation was capacitive, an alternating bias of 20/−20 V was applied with a pulse duration of 4 s across the gate electrodes. Simultaneously the fluorescence intensity was monitored with the photomultiplier tube (PMT) under the gate electrode that was kept grounded. The observed

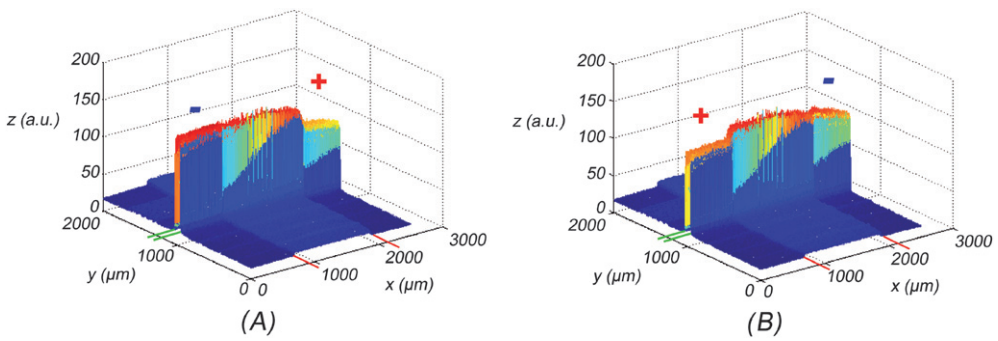


**Fig. 7** 3-Dimensional fluorescent intensity plots of the channel area during actuation. The green lines indicate the width of the channel and the red lines the inter-electrode space. The electrodes are located parallel to the *y*-axis. (A) A positive actuation voltage has been applied to the right-hand side electrode where the fluorescence has decreased. (B) A positive actuation voltage has been applied under the left-hand side electrode. Now fluorescence has decreased under this electrode.

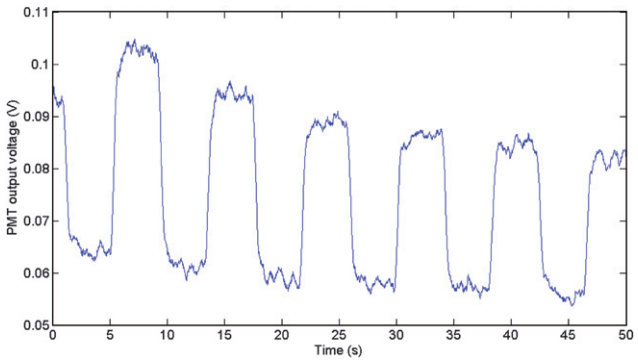


**Fig. 8** Fluorescent intensity changes measured by the photomultiplier tube (PMT) under a single electrode for an applied bias of +20/−20 V and a pulse duration of 4 s (frequency 0.125 Hz).

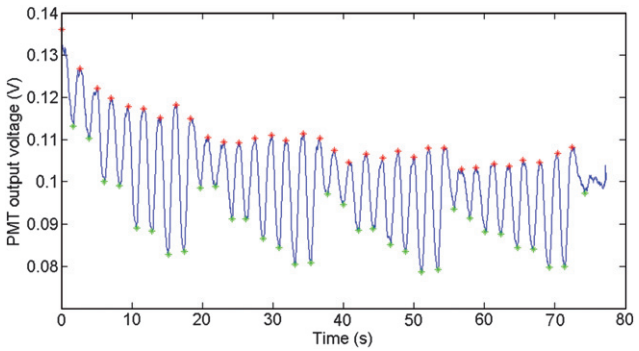


**Fig. 9** Fluorescence intensity as a function of time for a sequence of different applied bias potentials. Starting at $t = 0$, four times an actuation sequence of +/−10, +/−10, +/−15, +/−15, +/−20,+ /−20, +/−25, +/−25 V was applied. Red and green dots indicate, respectively, the fluorescence intensity maxima and minima during a potential period. The PMT output was filtered using a median filter with $n = 5$ to reduce the signal noise.

area was chosen close to the electrode gap. The output of the PMT is shown in Fig. 8. A distinct decrease and increase in intensity can be observed corresponding to positive and negative applied gate potentials, respectively. After each change of the gate potential the intensity reaches a constant value within 0.5 s, after which the continuing application of potential does not significantly contribute to a further intensity change. Since the capacitive pH actuation is transient while Faradaic processes are continuous, this indicates a capacitive actuation mechanism. The overall intensity furthermore shows a gradual exponential decrease, which we attributed to fluorescein photobleaching. The fluorescence intensity curve during actuation could be fitted successfully with an exponential function with a time constant of approximately 0.2 s. This time constant is comparable to the electrical time constant of 0.35 s observed in Fig. 6, but about a factor of 20 longer than the calculated RC time from the equivalent electrical circuit (0.012 s). At present we have only tentative explanations for this phenomenon. The most probable explanation is that buried charges in the silicon nitride delay the voltage application inside the solution. Another explanation is that slow kinetics for the exchange of potassium ions for protons in the first hydration layer, as observed in mica dissolution, could play a role.[30] The latter phenomenon, however, has not been observed at $Al_2O_3$ and $Ta_2O_5$ ISFET surfaces, where rapid protonation kinetics with response times of about 0.005 s were observed when the solution pH was changed.[31,32]

### Relation between gate potential and titrated amount of fluorescein

To establish the relation between the applied gate potential and the fluorescence intensity change, four sequences of bias potentials were applied where the potential was increased with increments of 5 V from 10 to 25 V for both positive and negative bias in pulse durations of 1 s. Fig. 9 shows the observed fluorescence intensity as a function of time. The PMT output was filtered using a median filter with $n = 5$ to reduce the signal noise.

To compensate for any changes in fluorescence intensity due to photobleaching of the fluorescent dye and for the background light, the fluorescence intensity change observed in Fig. 9 was converted to a relative intensity change by dividing through the (time-dependent) maximal intensity, $\Delta I_{rel} = (I_{max} - I_{min})/(I_{max} - I_{backgr})$.

The relative change in fluorescence intensity as a function of applied potential bias is plotted in Fig. 10. The data obtained for the fluorescein solution can be fitted by a straight line in the voltage regime studied, in accordance with the theoretical prediction of eqn (7) that the number of actuated protons is proportional to the applied voltage. At the maximum applied voltage of 25 V, the relative fluorescence intensity varies with 70%. An intensity variation of 70% around pH 6.9 (where the fluorescent dianion concentration is 0.061 mM) relative to the maximum fluorescence implies an oscillation between dianion concentrations of 0.094 mM and 0.028 mM. This means that 0.066 mM fluorescein is protonated when the applied potential changes with 25 V, which corresponds to a released proton amount of $5.5 \times 10^{-3}$ C m$^{-2}$. When the released amount of protons is calculated from the oxide model presented above using eqn (7), we find a value of $4.5 \times 10^{-3}$ C m$^{-2}$, which is in reasonable accordance. The relative change in intensity obtained

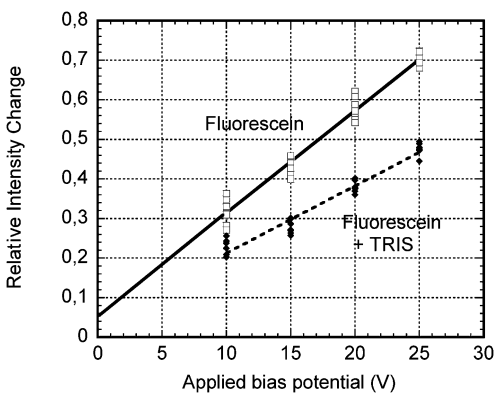


**Fig. 10** Relative change in fluorescence intensity amplitude as a function of the applied bias potential for a solution with 0.1 mM fluorescein and for a solution with 0.1 mM fluorescein and 0.1 mM TRIS. The linear fit through the fluorescein data points corresponds to the theoretically expected behavior. The line through the fluorescein + TRIS data points is meant only as a guide for the eye.

at 25 V corresponds to a pH oscillation of the electrolyte solution between pH 7.9 and 6.3 (approximately 1.6 pH units).

### Detecting the titration of other substances

A possible application of the proton actuation is the determination of the buffer capacity in small volumes, by using fluorescein as a pH indicator. In a preliminary measurement we determined the relative change in fluorescence intensity when 0.1 mM TRIS was added to the solution with 0.1 mM fluorescein. Fig. 10 shows that the addition of TRIS decreased the fluorescence amplitude from 70% to about 45%. In the observed volume of approximately 7 pL (radius 50 μm and height 860 nm) this fluorescence decrease will be due to the titration of about 100 amol of TRIS (0.015 mM) at the applied voltage amplitude of 25 V. Due to the uncertainty in the initial pH of the TRIS–fluorescein solution, a theoretical fit to the data points was not undertaken. This measurement indicates the potential of this method to determine the presence of very small quantities of acid or base.

### Further discussion and outlook

It is important to consider how the amount of protons released by this capacitive mechanism, which is about $4 \times 10^{-3}$ C m$^{-2}$ at 25 V actuation voltage, can be increased. Combining eqn (1) and (7) and substituting the breakdown field for *Vld*, we obtain as theoretical maximum for the amount of actuated protons

$$N_{\mathrm{H,max}} = E_{\mathrm{breakdown}} \varepsilon_0 \varepsilon_{\mathrm{r}} \frac{C_{\mathrm{buff}}}{\left(C_{\mathrm{buff}} + C_{\mathrm{DL}}\right)} \qquad (10)$$

The conclusion is that wall materials are preferred with a high breakdown field $E_{\mathrm{breakdown}}$, a high relative permittivity and a high proton buffer capacitance. Theoretically the last term of eqn (10) equaled 0.75 for the silicon nitride we used at the experimental pH and ionic strength, so that this term leaves little room for improvement. The field strength, however, can possibly be increased, since we operated the device at a field of maximally 0.07 V nm$^{-1}$, which is a factor of 9 lower than the breakdown field determined. Before insulator breakdown occurs, however, leakage currents were seen to occur, decreasing the capacitive character of the actuation. A thicker dielectric layer or a combination of different layers of dielectric could possibly decrease leakage currents and allow higher applied fields. Silicon nitride seems the best choice of material for a single layer since the dielectric strength we determined (600 MV m$^{-1}$) leaves practically no room for improvement. In conclusion we can state that with this capacitive method under the best circumstances it will be possible to actuate $4 \times 10^{-2}$ C m$^{-2}$ of protons. In a 1 μm high space this corresponds to a proton concentration change of 0.4 mM and in a 100 nm high space to a proton concentration change of 4 mM.

A general statement based on the findings of this research is that it is of major importance to be conscious of proton release and uptake from insulating walls in nanochannels when solution properties change or when gate voltages are applied in so-called ionic transistors. Generalizing this statement even further, we state the importance of taking account of the surface chemistry in nanofluidics.

The actuation method described here enables significant control of the pH in electrolyte solutions in very small volumes that does not rely on convection or diffusion. Due to its capacitive mechanism, it is a "soft" actuation method useful *e.g.* not only for bioassays or cell-based research, but also for detection in separation methods. The effect is largely independent of ionic strength enabling operation in physiological systems. Future developments could aim for improvements of the quality of the dielectric to enable higher applied fields and amounts of protons. The use of electrodes with a smaller surface area would furthermore enable a higher spatial resolution.

## References


1 J. C. T. Eijkel and A. van den Berg, Nanofluidics: what is it and what can we expect from it?, *Microfluid. Nanofluid.*, 2005, **1**(3), 249–267.
2 L. J. Bousse, N. F. de Rooij and P. Bergveld, Operation of chemically sensitive field-effect sensors as a function of the insulator–electrolyte interface, *IEEE Trans. Electron Devices*, 1983, **30**, 1263.
3 K. G. H. Janssen, H. T. Hoang, J. Floris, J. de Vries, N. R. Tas, J. C. T. Eijkel and T. Hankemeier, Solution titration by wall deprotonation during capillary filling of silicon oxide nanochannels, *Anal. Chem.*, 2008, **80**(21), 8095–8101.
4 R. Karnik, R. Fan, M. Yue, D. Y. Li, P. D. Yang and A. Majumdar, Electrostatic control of ions and molecules in nanofluidic transistors, *Nano Lett.*, 2005, **5**(5), 943–948.
5 R. B. M. Schasfoort, S. Schlautmann, L. Hendrikse and A. van den Berg, Field-effect flow control for microfabricated fluidic networks, *Science*, 1999, **286**(5441), 942–945.
6 R. E. G. van Hal, J. C. T. Eijkel and P. Bergveld, A general model to describe the electrostatic potential at electrolyte oxide interfaces, *Adv. Colloid Interface Sci.*, 1996, **69**, 31–62.
7 D. Bottenus, Y. J. Oh, S. M. Han and C. F. Ivory, Experimentally and theoretically observed native pH shifts in a nanochannel array, *Lab Chip*, 2009, **9**(2), 219–231.
8 M. A. Hayes, Extension of external voltage control of electroosmosis to high-pH buffers, *Anal. Chem.*, 1999, **71**(17), 3793–3798.
9 K. Ghowsi and R. J. Gale, Field-effect electroosmosis, *J. Chromatogr.*, 1991, **559**(1–2), 95–101.
10 E. J. van der Wouden, D. C. Hermes, J. G. E. Gardeniers and A. van den Berg, Directional flow induced by synchronized longitudinal and zeta-potential controlling AC-electrical fields, *Lab Chip*, 2006, **6**(10), 1300–1305.
11 Y.-J. Oh, D. Bottenus, C. F. Ivory and S. M. Han, Impact of leakage current and electrolysis on FET flow control and pH changes in nanofluidic channels, *Lab Chip*, 2009, **9**(11), 1609–1617.
12 W. Olthuis, B. H. van der Schoot, F. Chavez and P. Bergveld, A dipstick sensor for coulometric acid-base titrations, *Sens. Actuators*, 1989, **17**(1–2), 279–283.
13 B. van der Schoot and P. Bergveld, An ISFET-based microliter titrator—integration of a chemical sensor actuator system, *Sens. Actuators*, 1985, **8**(1), 11–22.
14 J. Luo, W. Olthuis, P. Bergveld, M. Bos and W. E. van der Linden, Determination of buffer capacity by means of an ISFET-based coulometric sensor actuator system with a gate-covering porous actuator, *Sens. Actuators, B*, 1994, **20**(1), 7–15.
15 P. Bergveld, Development of an ion-sensitive solid-state device for neurophysiological measurements, *IEEE Trans. Biomed. Eng.*, 1970, **BM17**(1), 70–71.
16 J. C. van Kerkhof, J. C. T. Eijkel and P. Bergveld, ISFET responses on a stepwise change in electrolyte concentration at constant pH, *Sens. Actuators, B*, 1994, **18**(1–3), 56–59.
17 R. J. Hunter, *Zeta Potential in Colloid Science: Principles and Applications*, Academic Press, London, 1981.
18 J. Lyklema, *Fundamentals of Interface and Colloid Science: Volume II: Solid–Liquid interfaces*, Academic Press, London, 1995.
19 C. S. Lee, W. C. Blanchard and C. T. Wu, Direct control of the electroosmosis in capillary zone electrophoresis by using an external electric-field, *Anal. Chem.*, 1990, **62**(14), 1550–1552.
20 L. Bousse and P. Bergveld, On the impedance of the silicon dioxide electrolyte interface, *J. Electroanal. Chem.*, 1983, **152**(1–2), 25–39.

21 D. L. Harame, L. J. Bousse, J. D. Shott and J. D. Meindl, Ion-sensing devices with silicon-nitride and borosilicate glass insulators, *IEEE Trans. Electron Devices*, 1987, **34**(8), 1700–1707.
22 M. N. Hamblin, J. M. Edwards, M. L. Lee, A. T. Woolley and A. R. Hawkins, Electroosmotic flow in vapor deposited silicon dioxide and nitride microchannels, *Biomicrofluidics*, 2007, **1**(3), 034101.
23 K. H. Bu and B. M. Moudgil, Selective chemical mechanical polishing using surfactants, *J. Electrochem. Soc.*, 2007, **154**(7), H631–H635.
24 L. Bousse and S. Mostarshed, The zeta-potential of silicon-nitride thin-films, *J. Electroanal. Chem.*, 1991, **302**(1–2), 269–274.
25 S. A. Smith and W. A. Pretorius, Spectrophotometric determination of p$K_a$ values for fluorescein using activity coefficient corrections, *Water SA*, 2002, **28**(4), 395–402.
26 S. A. Gajar and M. W. Geis, An ionic liquid-channel field-effect transistor, *J. Electrochem. Soc.*, 1992, **139**(10), 2833–2840.
27 H. O. Pierson, *Handbook of Chemical Vapor Deposition*, SciTech Publishing, Incorporated, 2nd edn, 1999.
28 M. Madou, *Fundamentals of Microfabrication—The Science of Miniaturization*, CRC, Boca Raton, Florida, 2nd edn, 2002.
29 L. Bousse, S. Mostarshed, D. Hafeman, M. Sartore, M. Adami and C. Nicolini, Investigation of carrier transport through silicon-wafers by photocurrent measurements, *J. Appl. Phys.*, 1994, **75**(8), 4000–4008.
30 N. Alcantar, J. Israelachvili and J. Boles, Forces and ionic transport between mica surfaces: implications for pressure solution, *Geochim. Cosmochim. Acta*, 2003, **67**(7), 1289–1304.
31 M. Klein, Time effects of ion-sensitive field-effect transistors, *Sens. Actuators*, 1989, **17**(1–2), 203–208.
32 B. H. van der Schoot, P. Bergveld, M. Bos and L. J. Bousse, The ISFET in analytical chemistry, *Sens. Actuators*, 1983, **4**(2), 267–272.

 